Lab on a Chip

PAPER

View Article Online
View Journal | View Issue

Cite this: *Lab Chip*, 2021, **21**, 608

Nanoporous silk films with capillary action and size-exclusion capacity for sensitive glucose determination in whole blood†

Augusto Márquez,[a] Moliria V. Santos,[b] Gonzalo Guirado,[c] Alex Moreno,[a] Salvador D. Aznar-Cervantes,[d] Jose Luis Cenis,[d] Silvia H. Santagneli,[e] Carlos Domínguez,[a] Fiorenzo G. Omenetto*[fghi] and Xavier Muñoz-Berbel*[a]

Received 9th July 2020,
Accepted 11th December 2020

DOI: 10.1039/d0lc00702a

rsc.li/loc

In optical biosensing, silk fibroin (SF) appears as a promising alternative where other materials, such as paper, find limitations. Besides its excellent optical properties and unmet capacity to stabilize biomacromolecules, SF in test strips exhibits additional functions, *i.e.* capillary pumping activity of 1.5 mm s^{-1}, capacity to filter blood cells thanks to its small, but tuneable, porosity and enhanced biosensing sensitivity. The bulk functionalization of SF with the enzymes glucose oxidase and peroxidase and the mediator ABTS produces colourless and transparent SF films that respond to blood glucose increasing 2.5 times the sensitivity of conventional ABTS-based assays. This enhanced sensitivity results from the formation of SF–ABTS complexes, where SF becomes part of the bioassay. Additionally, SF films triple the durability of most stable cellulose-based sensors. Although demonstrated for glucose, SF microfluidic test strips may incorporate other optical bioassays, *e.g.* immunoassays, with the aim of transferring them from central laboratories to the place of patient's care.

Introduction

Point of care (POC) devices are conceived to transfer medical tests from central laboratories to the place of patient's care. The flagship of POC devices is paper-based lateral flow assays (LFAs), where the paper[1] pumps the liquid through the system by capillarity, and the device provides the result after a few minutes and without user intervention. Albeit simple and low cost, most of the LFAs are restricted to yes/no or subjective and interpretable semi-quantitative results. Although sufficient in many situations, a quantitative result is necessary, for instance, in the monitoring of chronic patients. As an example, the level of glucose in diabetic patients is critical for decision-making. Quantitative LFAs should overcome the limitation of cellulose paper-based substrates, which are: (i) their opacity, with optical paths of a few microns, which are too short to perform absorbance measurements, and (ii) the ageing of the paper matrix, which discolours over time and produces colour inhomogeneity at the readout zone.

Alternatives based on nanocellulose paper, such as nanofibrillated paper[2] or bacterial cellulose,[3] and synthetic microfluidic paper manufactured from cyclic olefin copolymers (COCs)[4] or off-stoichiometry thiol–ene (OSTE) polymers[5] have been already produced overcoming some of the previous limitations. Nanocellulose paper, however, still relies on the random arrangement of cellulose nanofilaments, resulting in poorly transparent and variable optical systems.[6] Synthetic paper,[7] on the other hand, presents better optical properties and produces more reproducible and repetitive systems. Its main limitation is on the stability of the biomolecules, which is much shorter than that reported in cellulose-based systems.

In the pursuit of new materials for POC, silk fibroin (SF) from *Bombyx mori* has positioned as a real alternative to conventional cellulose-based paper in the development of microfluidic sensing platforms with optical transduction. SF is a natural protein fibre with chemical and thermal

[a] *Instituto de Microelectrónica de Barcelona (IMB-CNM, CSIC), Bellaterra, Barcelona, 08193, Spain. E-mail: xavier.munoz@imb-cnm; Tel: +34935947700*
[b] *São Carlos Institute of Physics, University of São Paulo, São Carlos, SP, Brazil*
[c] *Departament de Química, Universitat Autònoma de Barcelona Bellaterra (Barcelona), 08193, Spain*
[d] *Instituto Murciano de Investigación y Desarrollo Agrario y Alimentario (IMIDA), La Alberca (Murcia), 30150, Spain*
[e] *Institute of Chemistry, São Paulo State University (UNESP), Araraquara, SP, 14801-970, Brazil*
[f] *Silklab, Department of Biomedical Engineering, Tufts University, Medford, MA, 02155, USA. E-mail: fiorenzo.omenetto@tufts.edu*
[g] *Department of Electrical and Computer Engineering, Tufts University, Medford, MA, 02155, USA*
[h] *Department of Physics, Tufts University, Medford, MA, 02155, USA*
[i] *Laboratory for Living Devices, Tufts University, Medford, MA, 02155, USA*
† Electronic supplementary information (ESI) available. See DOI: 10.1039/d0lc00702a

stability,[8] mechanical robustness,[9] biocompatibility[10] and controllable biodegradability.[11] Natural SF fibres can be degummed, dissolved in water[12] and processed into a number of morphologies, including sponges, hydrogels, tubes, composites, microspheres or thin films. These matrices serve most notably as surgical sutures (*e.g.* SOFSILK™), carriers for drug delivery[13] and scaffolds for tissue engineering,[14] although also used as flexible interfacial components in electronic and photonic devices, such as edible food sensors[15] and organic light-emitting transistors.[16] Taking advantage of the excellent optical properties of SF (*i.e.* refractive index, RI, of 1.54,[17] and full transparency in the visible range), two- and three-dimensional optical components based on silk films have been already produced. These include diffractive patterns,[18] holograms,[19] optical grating,[20] waveguides[21] and photonic crystals.[22] Since SF films are obtained by crystallization under mild conditions (*i.e.* aqueous solutions, neutral pH, room temperature and vacuum), biomacromolecules such as cells, antibiotics, enzymes, monoclonal antibodies and peptides[23] can be incorporated in the bulk of the SF matrix, while preserving their structure and function for long times.[24,25]

This work studies the use of SF films in the development of optical/photonic microfluidic test strips for direct determination of analytes of clinical relevance in blood samples, here applied to glucose detection. It should be noted that, although immunochemical reactions are the most common bioassay implemented in cellulose-based test strips, an enzymatic bioassay for glucose detection has been selected here for: (i) simplifying the biomolecule stability test, which is performed through a simple enzymatic activity assay, and (ii) allowing the demonstration of the potential activity of SF films as active components of the biorecognition reaction, in this case through the reaction of SF with the ABTS mediator. In this article, the optical, structural, and microfluidic properties and the filtration capacity of SF films, either alone or bulk-modified with the components of the bioassay, are determined and compared. Optimal conditions are employed in the development of colorimetric silk-based POC systems for quantitative and sensitive determination of glucose in whole blood samples.

Experimental

Silk fibroin processing

Cocoons of *Bombyx mori*, obtained from silkworms reared in the sericulture facilities at IMIDA (Murcia, Spain), were chopped into 4 or 5 pieces and boiled in 0.02 M Na_2CO_3 (CAS number: 497-19-8; Sigma Aldrich) for 30 min to remove the glue-like sericin protein. Then, raw fibroin was rinsed thoroughly with water and dried at room temperature for 3 days. The extracted fibroin was dissolved in 9.3 M LiBr (CAS number: 7550-35-8, Acros Organics) for 3 h at 60 °C to generate a 20% w/v solution after dialyzing against distilled water for 3 days (Snakeskin Dialysis Tubing 3.5 kDa MWCO, Thermo Scientific) with eight total water exchanges. Thin films of SF were obtained after casting the solution in Petri dishes (Sigma Aldrich), overnight drying and crystallization after vacuum water annealing (*i.e.* 800 mbar; overnight) in a humid environment. Film functionalization with water soluble biomolecules, *i.e.* enzymes and mediators, was performed by incorporation of these compounds in the SF solution (direct dissolution of the lyophilized enzymes and solid mediator in the SF solution). In this work, the enzymes glucose oxidase from *Aspergillus niger* (GOx; EC 1.1.3.4; Sigma-Aldrich) and horseradish peroxidase (HRP; EC 1.11.1.7, Sigma-Aldrich) and the redox mediator 2,2′-azino-bis(3-ethylbenzothiazoline-6-sulfonic acid)diammonium salt (ABTS; CAS number: 30931-67-0; Sigma-Aldrich) were used. The drying/crystallization process in this case was exactly the same as that for pristine SF films.

Attenuated total reflectance-Fourier-transform infrared spectroscopy (ATR-FTIR) measurements

ATR-FTIR measurements were performed using a Platinum ATR (Alpha II spectrometer, Bruker) that contains a diamond crystal to measure attenuated total reflectance. Spectra were obtained by averaging 54 scans at a resolution of 4 cm^{-1} and are presented as $-\log(R/R_0)$, where R and R_0 are the reflectance values corresponding to the single beam spectra recorded for the sample and the reference, respectively. The reference was measured by simple exposure of the prism to air while the sample measurement was carried out by pressing the sample against the diamond prism.

Raman spectroscopy measurements

Raman spectra of the samples were collected on a Raman spectrometer (RAMII Bruker spectrometer, Bruker) equipped with a Ge detector using liquid nitrogen as the coolant and a Nd:YAG laser emitting at 1064 nm. The laser light power was 1000 mW. A back-scattering configuration was used. An average of 1024 scans was performed at a resolution of 4 cm^{-1} over a range from 4000 to 400 cm^{-1}.

X-Ray diffraction (XRD) measurements (theta–2theta scan)

XRD measurements were performed on a Materials Research Diffractometer (MRD; Malvern PANalytical Xpert Pro MRD, Malvern PANalytical). The diffractometer had a horizontal omega–2theta goniometer (320 mm radius) in a four-circle geometry and it worked with a ceramic X-ray tube with a Cu Kα anode (l = 1.540598 Å). The detector used was the Pixel, a fast X-ray detector based on Medipix2 technology. Incident optics used included: a parabolic mirror; a divergent slit, 1/4°; a mask, 2 mm; Soller slits, 0.04 rad; and a Ni filter (0.02 mm). Diffracted optics used included: the Pixel detector and an antiscatter slit, 7.5 mm. The measurements were performed using the scanning mode of the detector. Measurement conditions: 2theta range = 10–50°; step size = 0.03°; and counting time (time per step) = 500 s.

Thermogravimetric analysis (TGA)

Thermogravimetric analysis was performed with a thermal analysis system (STA 449 F1 Jupiter, Netzsch) controlled using Netzsch software. Experimentally, 5 mg samples of SF were deposited in an Al_2O_3 crucible and heated up from RT to 700 °C at a ramp of 10 °C min^{-1} while the loss of mass was registered.

UV-vis spectroscopy

A simple setup including a deuterium–halogen lamp (DH-2000-BAL, Ocean Optics) as a light source, a spectrometer (QEPro, Ocean Optics) and a custom-made PMMA sample holder with SMA optic fibres (230 μm cladding; 200 μm core; numerical aperture 0.22; Thorlabs) connections was used. The sample holder left a space of 2 mm between the optic fibres for insertion of the sample cartridge. Directly after the addition of the sample into the well of the sample carrier, this was introduced in the space between the fibres to initiate the absorbance measurements.

Spectroelectrochemical measurements

A spectroelectrochemical apparatus (SPELEC, Dropsens) controlled using DROPVIEW SPELEC Software (Dropsens) was used to measure simultaneously cyclic voltammetry and the absorption spectra of functionalized SF pads of 4 mm in diameter. The SF pads were positioned on commercial electrodes (P10, Dropsens) containing a transparent working electrode of poly(3,4-ethylenedioxythiophene) (PEDOT). A 50 μL drop of phosphate buffered saline (PBS) solution with or without glucose was dispensed onto the pad and the Teflon chamber was closed to start the measurements. The PBS composition was as follows: 137 mM NaCl (CAS number: 7647-14-5, Sigma Aldrich), 2.7 mM KCl (CAS number: 7447-40-7, Sigma Aldrich), 10 mM Na_2HPO_4 (CAS number: 7558-79-4, Sigma Aldrich) and 1.8 mM KH_2PO_4 (CAS number: 7778-77-0, Sigma Aldrich).

Porosity measurements

The specific surface area, porosity and pore size were measured by the N_2 adsorption-BET (Brunauer–Emmett–Teller) method with an accelerated surface area and porosimetry system using nitrogen as the adsorption/desorption gas (ASAP 2020, Micromeritics). The samples were pre-treated with a degassing step for 20 h at 120 °C.

Materials mechanization

PMMA foil (Goodfellow) of 0.5 mm was cut using a CO_2 laser ablation system (Epilog mini 24, EpilogLaser). SF films were cut into 4 mm circles using a plotter instrument (CAMM-1 Servo Cutter Plotter, Roland).

Capillary pumping experiments

SF layers were cut into 2 × 30 mm pieces and located in a PMMA structure that contained a well to load the colorant and a channel to hold the SF film. The well of 4 mm in diameter and 200 μm in depth was filled with the colorant solution and the liquid behaviour was observed both in the presence and absence of the SF film in the channel.

Freeze drying

SF solutions of different concentrations were cast on Petri dishes and frozen at −20 °C. Then, they were translated to a freeze dryer (Lyo-works Benchtop Freeze Dryer, LabConco) and exposed to a 0.01 mbar atmosphere at −80 °C for 12 h.

Blood samples

For the whole blood measurements, defibrinated sheep blood (Remel animal blood purchased in Sigma-Aldrich) was used. The Remel animal blood meets all standards for laboratory tests. The glucose concentration in the defibrinated blood was determined using tests strips (Accu-Chek, Roche Diagnostics), as the average of three consecutive determinations. In the calibration with blood samples, the glucose concentration was adjusted to different values. To this end, the necessary amount of glucose to increase the concentration to the desired magnitude was determined considering the initial glucose concentration, and then dissolved in the suitable amount of blood.

Image analysis

Pictures of the SF functionalized films were analysed using public domain ImageJ software. The average values of RGB were obtained from the pixels that comprise the selected area of the picture (*i.e.* SF film).

Statistical analysis

Experimental data from the studies were subjected to statistical analysis, and expressed as mean ± standard deviation (SD), unless another terminology is stated. Origin Software® (v.9.0, OriginLab) was used with an empirical distribution with averaging for the quantile interpolation.

Results and discussion

Characterization of doped and pristine silk fibroin films

Crystalline SF films (10 μm thick) were obtained after drying and vacuum annealing at room temperature of aqueous SF solutions under the experimental conditions detailed in ref. 12. The crystallization protocol was completely green and water-based, and allowed the incorporation of water-soluble biomolecules in the SF matrix, *e.g.* enzymes, while preserving their structure and function. In this case, the water-soluble enzymes GOx and HRP and the redox mediator ABTS were incorporated in the SF matrix. First, suitable amounts of enzymes and mediator were weighed and directly dissolved in the aqueous solution of SF to avoid the dilution of the silk. Then the solution was deposited on a substrate, dried and crystallized as described by the pristine SF films. The concentrations of enzymes and mediator in the SF were

selected from an optimization protocol (see Fig. S6 in the ESI†) and set at 25 μg ml^{-1} for GOx, 60 μg ml^{-1} for HRP and 90 μg ml^{-1} for ABTS. The presence of both enzymes and the mediator endowed the SF films with sensitivity to glucose.

The SF films presented high transparency, either pristine (Fig. 1a) or when doped with enzymes (Fig. 1b), with transmittances in the visible range always above 90% (Fig. 1c). The absorption below 300 nm was attributed to the π → π* transition of the amino acids (*i.e.* tyrosine and phenylalanine) present in the SF molecular chain.[26] Besides, doped SF films presented an additional absorption band at 420 nm associated with HRP. None of these bands interfered in the colorimetric detection of glucose in whole blood.

The biomolecule doping slightly modified the structure and properties of the SF films. The transition from an amorphous to a crystalline structure of the SF has been widely studied by infrared spectroscopy[24,27,28] and essentially attributed to an enhancement in the β-sheet contribution to the amide I band (1600–1700 cm^{-1}). While the non-annealed SF presented an amide I band centred at around 1640 cm^{-1}, which was assigned to random-coil structures, in the annealed samples the band peak shifted to 1620 cm^{-1} (Fig. 1d), which was attributed to the β-sheet conformation. An additional β-sheet signal was recorded at 1700 cm^{-1} likewise a higher relative contribution of the tyrosine side chain in the amide II at 1514 cm^{-1}, related to the packing of the β-sheet crystals.[29] All this evidence of β-sheet formation by SF crystallization was still present, but diminished, in the presence of enzymes and mediators.

X-ray diffraction studies[30] confirmed the structural changes associated with biomolecule doping. The pristine SF films showed diffraction peaks corresponding to the α-helix structure at 11.95° (lattice spacing, d = 0.740 nm) and 24.02° (0.370 nm), and to the β-sheet structure at 16.71° (0.530 nm), 20.34° (0.436 nm), 24.49° (0.363 nm), 30.90 (0.289 nm) and 34.59° (0.259 nm) (Fig. 1e). The addition of enzymes into the SF matrix caused a remarkable change in the diffraction profile, especially in the α-helix peaks that almost disappeared. This change may be attributed to the entrapment of water-soluble enzymes in the hydrophilic α-helix regions, which produced a partial loss of crystallinity. It was not possible to identify additional diffraction peaks associated with the presence of protein crystals. This result suggested that enzymes either did not crystallize inside the SF film or produced signals that were too weak to be detected.

The presence of the biomolecules also modified the thermal stability of the sample (Fig. 1f). The thermogravimetric records of the SF films presented two regions, one below 150 °C attributed to the removal of physisorbed water and the second one, in the range between 200 and 650 °C, associated with the degradation of SF β-sheet regions.[29,31] The SF films containing enzymes maintained a higher water content after vacuum annealing (around 1% in weight) and became slightly less resistant to temperature, presenting a faster degradation profile by the lower thermal stability of biomolecules. Nevertheless, this stability loss did not compromise the performance of the biosensor.

Silk fibroin as an active biosensing matrix

From a functional point of view, the bulk incorporation of GOx, HRP and ABTS into the SF matrix endowed it with sensitivity to glucose molecules. Importantly, SF was not only the support material where the bioassay took place, but also it had an active role as the microfluidic platform, size-exclusion filter and reagent of the bioassay. Regarding the latter, the biosensing mechanism, shown in Fig. 2a, took

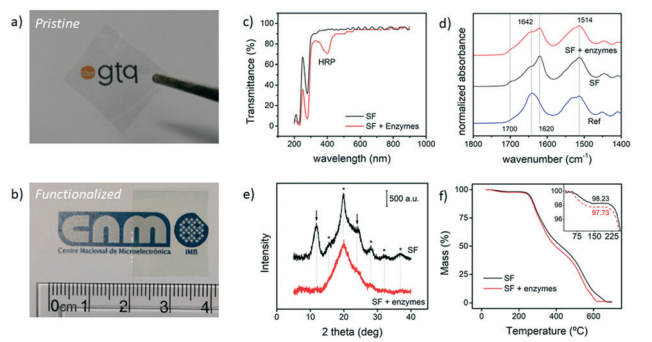

Fig. 1 SF film characterization. Pictures of a) pristine and b) doped SF films. c) UV-vis-NIR transmittance spectra, d) ATR-FTIR spectra, e) X-ray diffraction patterns and f) thermogravimetric analysis of 100% w/v SF layers and SF layers doped with 4% w/w glucose oxidase and 6% w/w horseradish peroxidase. In figure d, the reference spectrum refers to a non-annealed SF film.

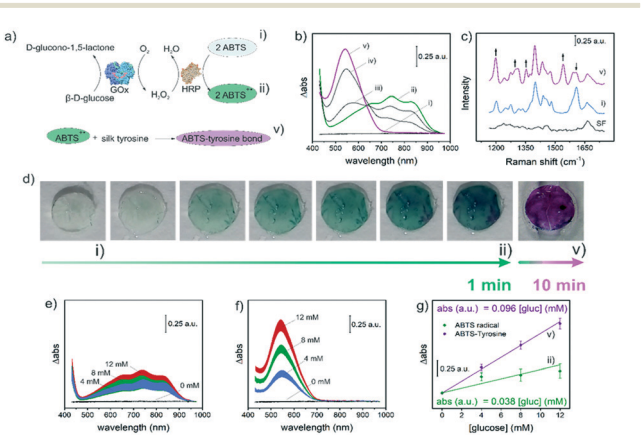

Fig. 2 Biosensor principle: ABTS radical generation and self-reaction with the SF matrix. a) Scheme of the enzymatic reaction for glucose determination. b) Absorption spectra i) before and ii) 75, iii) 130, iv) 300 and v) 900 s after the functionalized SF is soaked by capillary pumping with a 12 mM glucose PBS solution. c) Normalized Raman spectra of the SF films (Ref) and doped SF films i) before and v) after the complete reaction with glucose in PBS. d) Pictures of the doped SF film colour change induced by wetting with a PBS 12 mM glucose solution. Average absorption spectra of functionalized SF e) 75 s and f) 900 s after the addition of PBS solutions with different glucose concentrations. g) Calibration curves for PBS glucose solutions using the ABTS radical signal ii) at 745 nm or the ABTS–tyrosine signal v) at 545 nm (n = 5).

benefit from the interaction between ABTS and proteins reported by Åkerström *et al.*[32]

Briefly, the bio-functionalized SF films responded to glucose through a conventional cascade enzymatic reaction, where the redox mediator ABTS was finally oxidized to its green radical ion form (Fig. 2a, ii). This compound presented multiple absorption bands in the visible range susceptible to optical analysis, with the band at 735 nm being the most intense one (Fig. 2b, ii). In a second step, ABTS radicals reacted with the tyrosine amino acids from the SF matrix to produce a purple SF–ABTS complex (Fig. 2a, v). The complex presented a single absorption band at 545 nm that doubled the intensity of the most intense bands corresponding to ABTS (Fig. 2b, iii to v). The formation of the SF–ABTS complex increased 2.5 times the sensitivity of the assay (0.038 *versus* 0.096 A.U. mM^{-1} for the ABTS radical ion and the SF–ABTS complex, respectively, Fig. 2g) and expanded the linear range of the bioassay, enabling us to distinguish between hypoglycemic (4 mM glucose), pre-diabetic (8 mM) and diabetic (12 mM) patients (compare Fig. 2e corresponding to ABTS with Fig. 2f considering the SF–ABTS complex formation).

SF–ABTS complex formation involved the reduction of tyrosine amino acids and their covalent bonding to the ABTS radical ion. This mechanism was evidenced by ATR-FTIR (see details in ESI.1†) and corroborated by Raman spectroscopy, which showed alterations in the bands corresponding to carbon and nitrogen bonds (Fig. 2c). Concretely, Raman spectroscopy revealed the appearance of signals corresponding to C–C aliphatic symmetric stretching vibrations at 1200, 1300 and 1350 cm^{-1} and N=N symmetric stretching vibrations at 1540 cm^{-1} after reaction with glucose, while C–N symmetric stretching vibrations at 1610 cm^{-1} disappeared.[33,34] The absorption spectrum of the resulting SF–ABTS complex was independent of the applied voltage (see spectroelectrochemical analysis of SF–ABTS complexes in ESI.2†), indicating that ABTS lost its redox capacity after breakage and bonding to the tyrosine residues of SF. This was important since the reaction stopped after 10 min for the formation of SF–ABTS complexes, providing quantitative results that remained unaltered over time (time-independent), in opposition to conventional time-dependent enzymatic assays (see kinetic evolution of the absorption signal after reaction with glucose in ESI.3†).

Silk fibroin film microstructure and fluid management

SF films implemented in test strips demonstrated capillary pumping activity and capacity to filter blood cells. The porosity of the SF is related to the annealing process in terms of structure compression, as shown through XRD analysis. The annealing process reduced the water content of the films by vacuum exposure. To demonstrate this, SF solutions containing 1 to 20% w/v SF in water were prepared, freeze-dried and annealed. The resulting SF films were imaged by

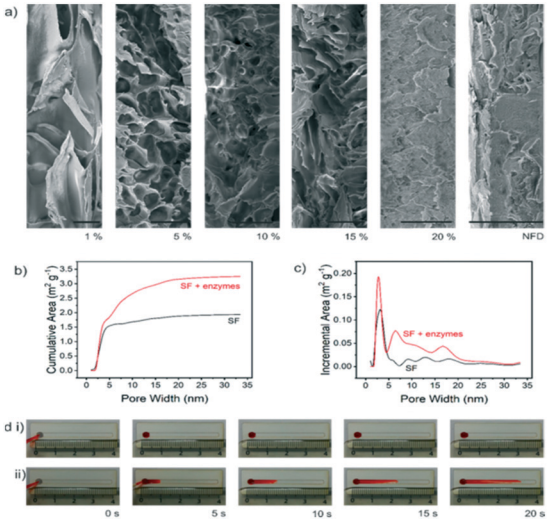

Fig. 3 SF microstructure and capillary pumping properties. a) SEM images of freeze-dried cast SF solutions of different concentrations in w/v (1 to 20%) after water annealing and SEM image of a non-freeze-dried (NFD) film, generated by casting and drying at RT (scale bar of 20 μm in every case). b) Surface area measurement (cumulative area) and c) pore size distribution (by incremental area) for the pristine and enzyme-doped SF films. Comparison between PMMA structures without d.i) and with d.ii) a SF film located in the channel, demonstrating the capillary pumping properties of the structure.

SEM to qualitatively evaluate the surface porosity of the SF films (Fig. 3a). It was apparent from the images that SF films with a higher water content, prior to the freeze-drying process, showed a higher porosity and larger pore size. A SEM image of a non-freeze-dried (NFD) film is also presented for the sake of comparison. This film, expected to retain only <2% of water content (see TGA results in Fig. 1f), showed a very dense aspect and an average pore diameter of 6.3 nm for pristine and 6.8 nm for doped SF films (by BET analysis). The pore diameter distribution was located below 20 nm for both pristine and doped SF films.

A higher surface area was observed in the case of the enzyme-doped films (3.2 m^2 g^{-1}), when compared to the pristine films (1.9 m^2 g^{-1}) (Fig. 3b). Although the average pore size was barely affected, a higher contribution was observed for the pore size region between 5 and 20 nm for the doped films (Fig. 3c), suggesting that the enzymes generated defects in the material, increasing locally the surface area and the pore size.

Additionally, it was also proved that particles larger than 1 μm could not penetrate the film (demonstrated by the bacterium *Escherichia coli*; ESI.4†), which are much smaller than any blood cells in the sample (6–8 μm). The observed SF structure is very relevant for real sample analysis, as it permitted whole cells from the bulk of the material to be retained. This porosity, together with its dual hydrophobic (by the presence of β-sheet domains) and hydrophilic nature (due to α-helix regions), endowed the SF films with capillary pumping capacity. Additionally, it was already proved that the water content in the initial SF solution determined, in part, the final porosity of the SF films. SF samples containing

between 5 and 10% fibroin produced highly porous films after freeze-drying and water annealing, with micrometric porous sizes even evident in SEM observation. This possibility of modifying the porosity of the films may be of great importance in the development of other types of biosensors, *e.g.* immunochemical, where larger cavities may be necessary for the recognition reaction. It should be remarked, however, that it is just a preliminary study on porosity modulation and a more extensive evaluation and optimization will be necessary to achieve precise tuning of the silk film microstructure.

Regarding capillarity, in Fig. 3d it is clearly observed how the polymeric test strips, initially too hydrophobic to present capillarity, pumped the liquid when modified with SF films (see the video in the ESI†). The recorded front flow velocity of 1.5 mm s^{-1} was comparable to those of reported microfluidic synthetic paper (between 1.7 and 2 mm s^{-1}),[5] polymer micropillar arrays (4 mm s^{-1} in serum)[35] or cellulose-based strips (1.6 mm s^{-1} for blood in nitrocellulose).[36]

Glucose analysis in whole blood

Test strips were designed and fabricated by laser ablation in PMMA (see ESI.5† for details). In the measurement, 4 μl of whole blood was loaded into the well of the strip (Fig. 4a, i). The functionalized SF film was brought into contact with the sample by the edge and, by capillarity, pumped the plasma through the SF matrix while maintaining the cell fraction into the well (Fig. 4a, ii). Blood glucose reacted with the enzymes and the mediator changed from uncoloured to deep purple by the formation of the SF–ABTS complex (Fig. 4a, iii), which was detected optically after insertion into the holder (ESI.5†).

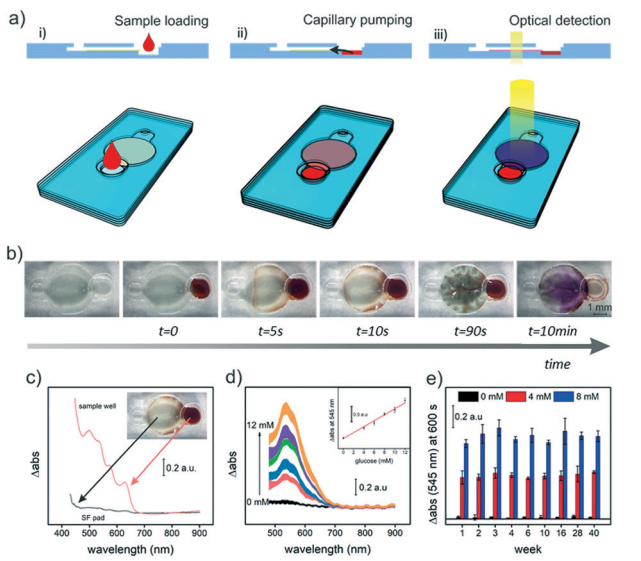

Fig. 4 Whole blood filtration and glucose quantification. a) Scheme of the PMMA test strip (cross-section and 3D) for SF positioning and analyte measurement. The sample is loaded into the well i), the pad is wetted by capillary pumping ii) and the SF colour change is detected iii). b) Pictures of the top view of the test strip illustrating the whole process depicted in a). c) Absorption spectra of the blood charged into the well of the prototype and a SF pad wetted by capillary pumping with whole blood. The spectra correspond to blood samples with a 4 mM glucose concentration 60 s after the infusion of the sample. d) Absorption spectra of the silk pads 600 s after the addition of whole blood (4 mM) and glucose spiked whole blood samples at 6, 8, 10 and 12 mM and calibration curve using the absorbance values at 545 nm. e) Durability of the biosensors presented as the average response (absorbance increment at 545 nm) of the pads to 0, 4 and 8 mM glucose PBS solution in time (n = 5).

Sequential photographs of the test strip after blood addition are depicted in Fig. 4b. Over time, blood was filtered and plasma started to diffuse by capillarity from the well to the detection area in less than 10 s. After 90 s, the green colour associated with ABTS appeared, which became purple by the reaction with the silk matrix. After 10 min of reaction, only dried blood cells remained in the well by the transport of the plasma through the silk film, bringing to the well a light brownish colour. Thanks to the filtering capacity of the SF pads, the interference associated with the presence of haemoglobin in red cells was largely minimized (Fig. 4c). After optimization of the SF film composition (see ESI.6†), it was possible to determine the glucose concentration in spiked whole blood samples with precision and sensitivity in the range from 0 to 12 mM (Fig. 4d) using a deuterium–halogen lamp (DH-2000-BAL, Ocean Optics) as a light source and a spectrometer (QEPro, Ocean Optics). The SF pads presented high reproducibility with a variation coefficient always below 10%, improving the variation reported in paper-based test strips commonly between 15 and 20%.[37,38] The sample volume, comparable to those of commercial test strips, was liable to be reduced by decreasing the volume of the well and/or the diameter of the SF film (currently 4 mm). Current whole blood analysis was performed with defibrinated samples, although comparable to real *in situ* analysis since the duration of the assay was not long enough to produce a remarkable coagulation. In accordance with the RE-ASSURED (real-time, easy sample collection, affordable, sensitive, specific, user-friendly, rapid and robust, equipment-free and deliverable to end-users) criteria[39] for diagnostics in resource-constrained environments, comparable results were obtained when, instead of laboratory instrumentation, SF test strips were analysed with a smartphone and image analysis with the freeware ImageJ (see details in ESI.7†).

Besides, the enzymes and ABTS immobilized within the SF matrix presented extraordinary long-term stability and unmet durability, maintaining the same response to glucose concentrations, *i.e.* 0, 4 and 8 mM, after 40 weeks of dry storage at room temperature (Fig. 4e). It is important to remark that storage was performed in the dark to avoid light-induced ABTS oxidation. This stability of bio-components bulk immobilized in the SF films widely surpassed that reported for most durable cellulose-based test strips in the market, *i.e.* Onetouch, Agamatrix or Nipro Diagnosis, which did not exceed 4 months, even when refrigerated.

Conclusions

In summary, we have developed a microfluidic platform for optical biosensing based on bio-functionalized SF films, taking advantage of the optical and biocompatible properties of the latter. The use of enzyme-doped SF films as a sensitive matrix for glucose detection is presented, highlighting as a novelty the capability of the material to filter blood cells, to pump liquids through its nanoporous matrix without the need for external instruments and to increase 2.5 times the sensitivity of glucose determination by reaction of the SF matrix components with molecules resulting from the enzymatic reaction. These advantages, together with the already reported green and water-based processing, long-term stability of biomolecules (triple that of most durable cellulose-based strips) and high transparency in the visible range, make SF pads ideal for colorimetric detection of biomarkers at the POC. Glucose is here detected with precision, sensitivity and in a wide linear range enabling us to distinguish from hypoglycemic and hyperglycemic states of a diabetic patient by a simple and inexpensive image analysis. Moreover, and in accordance with the RE-ASSURED criteria for diagnosis in resource-constrained environments, fast analysis can be achieved by simple imaging with a smartphone, or even with the naked eye. Although proven in glucose, many other laboratory bioassays requiring optical analysis of biomarkers in whole blood may be implemented in the current SF-based platform and translated from the laboratory to the point of care.

Conflicts of interest

There are no conflicts to declare.

Acknowledgements

This work was supported by the Spanish R & D National Program (MICINN: Project TEC2014-54449-C3-1-R and RTI2018-100773-B-C31). Moliria Vieira dos Santos acknowledges FAPESP for a postdoctoral fellowship, grants #2016/11591-8 and #2018/11039-9. A. M. is also grateful to MICINN for the award of a research studentship from the FPI program (BES-2015-072946).

Notes and references

1 J. Hu, S. Q. Wang, L. Wang, F. Li, B. Pingguan-Murphy, T. J. Lu and F. Xu, *Biosens. Bioelectron.*, 2014, **54**, 585–597.
2 J. I. Morán, V. A. Alvarez, V. P. Cyras and A. Vázquez, *Cellulose*, 2008, **15**, 149–159.
3 S. Ummartyotin, J. Juntaro, M. Sain and H. Manuspiya, *Ind. Crops Prod*, 2012, **35**, 92–97.
4 B.-Y. Pemg, C.-W. Wu, Y.-K. Shen and Y. Lin, *Polym. Adv. Technol.*, 2010, **21**, 457–466.
5 J. Hansson, H. Yasuga, T. Haraldsson and W. Van Der Wijngaart, *Lab Chip*, 2016, **16**, 298–304.
6 L. Hu, G. Zheng, J. Yao, N. Liu, B. Weil, M. Eskilsson, E. Karabulut, Z. Ruan, S. Fan, J. T. Bloking, M. D. McGehee, L. Wågberg and Y. Cui, *Energy Environ. Sci.*, 2013, **6**, 513–518.
7 C. F. Carlborg, T. Haraldsson, K. Öberg, M. Malkoch and W. van der Wijngaart, *Lab Chip*, 2011, **11**, 3136–3147.
8 I. C. Um, H. Kweon, Y. H. Park and S. Hudson, *Int. J. Biol. Macromol.*, 2001, **29**, 91–97.
9 L.-D. Koh, Y. Cheng, C.-P. Teng, Y.-W. Khin, X.-J. Loh, S.-Y. Tee, M. Low, E. Ye, H.-D. Yu, Y.-W. Zhang and M.-Y. Han, *Prog. Polym. Sci.*, 2015, **46**, 86–110.
10 Y. Yang, X. Chen, F. Ding, P. Zhang, J. Liu and X. Gu, *Biomaterials*, 2007, **28**, 1643–1652.
11 Y. Cao and B. Wang, *Int. J. Mol. Sci.*, 2009, **10**, 1514–1524.
12 D. N. Rockwood, R. C. Preda, T. Yücel, X. Wang, M. L. Lovett and D. L. Kaplan, *Nat. Protoc.*, 2011, **6**, 1612–1631.
13 T. Yucel, M. L. Lovett and D. L. Kaplan, *J. Controlled Release*, 2014, **190**, 381–397.
14 E. S. Gil, B. B. Mandal, S.-H. Park, J. K. Marchant, F. G. Omenetto and D. L. Kaplan, *Biomaterials*, 2010, **31**, 8953–8963.
15 H. Tao, M. A. Brenckle, M. Yang, J. Zhang, M. Liu, S. M. Siebert, R. D. Averitt, M. S. Mannoor, M. C. McAlpine, J. A. Rogers, D. L. Kaplan and F. G. Omenetto, *Adv. Mater.*, 2012, **24**, 993–993.
16 R. Capelli, J. J. Amsden, G. Generali, S. Toffanin, V. Benfenati, M. Muccini, D. L. Kaplan, F. G. Omenetto and R. Zamboni, *Org. Electron.*, 2011, **12**, 1146–1151.
17 M. B. Applegate, G. Perotto, D. L. Kaplan and F. G. Omenetto, *Biomed. Opt. Express*, 2015, **6**, 4221–4227.
18 H. Perry, A. Gopinath, D. L. Kaplan, L. Dal Negro and F. G. Omenetto, *Adv. Mater.*, 2008, **20**, 3070–3072.
19 M. Cronin-Golomb, A. R. Murphy, J. P. Mondia, D. L. Kaplan and F. G. Omenetto, *J. Polym. Sci., Part B: Polym. Phys.*, 2012, **50**, 257–262.
20 J. J. Amsden, P. Domachuk, A. Gopinath, R. D. White, L. D. Negro, D. L. Kaplan and F. G. Omenetto, *Adv. Mater.*, 2010, **22**, 1746–1749.
21 S. T. Parker, P. Domachuk, J. Amsden, J. Bressner, J. A. Lewis, D. L. Kaplan and F. G. Omenetto, *Adv. Mater.*, 2009, **21**, 2411–2415.
22 Y. Wang, W. Li, M. Li, S. Zhao, F. De Ferrari, M. Liscidini and F. G. Omenetto, *Adv. Mater.*, 2019, **31**, 1805312.
23 A. B. Li, J. A. Kluge, N. A. Guziewicz, F. G. Omenetto and D. L. Kaplan, *J. Controlled Release*, 2015, **219**, 416–430.
24 B. D. Lawrence, M. Cronin-Golomb, I. Georgakoudi, D. L. Kaplan and F. G. Omenetto, *Biomacromolecules*, 2008, **9**, 1214–1220.
25 Y. Liu, H. Liu, J. Qian, J. Deng and T. Yu, *Anal. Chim. Acta*, 1995, **316**, 65–72.
26 G. Perotto, Y. Zhang, D. Naskar, N. Patel, D. L. Kaplan, S. C. Kundu and F. G. Omenetto, *Appl. Phys. Lett.*, 2017, **111**, 103702.
27 Q. Lu, X. Hu, X. Wang, J. A. Kluge, S. Lu, P. Cebe and D. L. Kaplan, *Acta Biomater.*, 2010, **6**, 1380–1387.
28 J. Park, S.-G. Lee, B. Marelli, M. Lee, T. Kim, H.-K. Oh, H. Jeon, F. G. Omenetto and S. Kim, *RSC Adv.*, 2016, **6**, 39330–39334.
29 X. Hu, K. Shmelev, L. Sun, E. S. Gil, S. H. Park, P. Cebe and D. L. Kaplan, *Biomacromolecules*, 2011, **12**, 1686–1696.

30 M. Li, W. Tao, S. Kuga and Y. Nishiyama, *Polym. Adv. Technol.*, 2003, **14**, 694–698.
31 M. V. Santos, É. Pecoraro, S. H. Santagneli, A. L. Moura, M. Cavicchioli, V. Jerez, L. A. Rocha, L. F. C. De Oliveira, A. S. L. Gomes, C. B. De Araújo and S. J. L. Ribeiro, *J. Mater. Chem. C*, 2018, **6**, 2712–2723.
32 B. Åkerström, G. J. Maghzal, C. C. Winterbourn and A. J. Kettle, *J. Biol. Chem.*, 2007, **282**, 31493–31503.
33 P. Monti, G. Freddi, S. Sampaio, M. Tsukada and P. Taddei, *J. Mol. Struct.*, 2005, **744–747**, 685–690.
34 P. Monti, G. Freddi, A. Bertoluzza, N. Kasai and M. Tsukada, *J. Raman Spectrosc.*, 1998, **29**, 297–304.
35 C. Jönsson, M. Aronsson, G. Rundström, C. Pettersson, I. Mendel-Hartvig, J. Bakker, E. Martinsson, B. Liedberg, B. MacCraith, O. Öhman and J. Melin, *Lab Chip*, 2008, **8**, 1191.
36 H. Li, D. Han, G. M. Pauletti and A. J. Steckl, *Lab Chip*, 2014, **14**, 4035–4041.
37 T. Ji, X. Xu, X. Wang, Q. Zhou, W. Ding, B. Chen, X. Guo, Y. Hao and G. Chen, *Sens. Actuators, B*, 2019, **282**, 309–316.
38 B. O'Farrell, in *Lateral Flow Immunoassay*, Humana Press, 2009, pp. 1–33.
39 K. J. Land, D. I. Boeras, X. S. Chen, A. R. Ramsay and R. W. Peeling, *Nat. Microbiol.*, 2019, **4**, 46–54.